Four Terminal Electrochemistry: A Back-Gate Controls the Electrochemical Potential of a 2D Working Electrode

Yuxin Wang[a] and C. Daniel Frisbie*[,a,b]

[a]Department of Chemistry, University of Minnesota, 207 Pleasant St SE, Minneapolis, MN 55455 USA and [b]Department of Chemical Engineering and Materials Science, University of Minnesota, 421 Washington Ave SE, Minneapolis, MN 55455 USA

Abstract

We demonstrate that ultrathin semiconductor working electrodes integrated into metal/insulator/semiconductor (MIS) stacks are an enabling platform for understanding non-Faradaic semiconductor electrochemistry. Here, 5 nm thick ZnO electrodes were deposited on 50 nm HfO_2 dielectric on a Pd 'gate' electrode. Application of a bias V_G between the Pd gate and the ZnO causes electrons to accumulate in the ZnO as measured by recording the ZnO in-plane sheet conductance. By contacting the top surface of the ZnO layer with electrolyte in a conventional three-electrode electrochemical cell, we show that the gate voltage V_G modulates the electrochemical potential V_{ZnO} of the ZnO film with respect to a reference electrode. Electrochemical potential changes ΔV_{ZnO} up to -1 V vs Ag/Ag^+ are achieved for V_G = +7 V. Furthermore, by measuring V_{ZnO} vs. V_G, we extract the quantum capacitance C_Q of the ZnO film as a function of Fermi level position, which provides a direct measure of the ZnO electronic density of states (DOS). Finally, we demonstrate that the gated ZnO working electrodes can disentangle the two principal components of electrochemical potential, namely the Fermi level shift $\Delta\delta$ and the double layer charging energy $e\Delta\phi_{EDL}$. This disentanglement hinges on a fundamental difference between back-gating and normal electrochemical control, namely that electrochemical control requires double layer charging while back-gate control does not. Collectively, the results show that the backside gate electrode is an effective fourth terminal that enables measurements that are difficult to achieve in conventional three-terminal electrochemical setups.

Keywords: 2D semiconductor, ZnO, quantum capacitance, electrochemical potential, double layer

* Corresponding author: frisbie@umn.edu

Introduction

In recent work we have demonstrated that the electric field effect can enhance the kinetics of electrochemical reactions at 2D semiconductor working electrodes.[1-3] The essential concept is to integrate an ultrathin semiconductor electrode into a metal/insulator/semiconductor (MIS) stack. The 2D semiconductor layer at the top of the stack is the working electrode in a typical three electrode electrochemical setup, Figure 1a, and the metal at the back of stack, called the "gate", serves as an independently controlled fourth electrode. Because the semiconductor and gate are capacitively coupled in the MIS stack, a voltage V_G applied between them results in electron accumulation or depletion in the semiconductor, depending on the sign and magnitude of V_G. Importantly, the gate-induced electron density in the semiconductor occurs independently of, and in summation with, the electron accumulation or depletion caused by the electrochemical potential V_W applied between the semiconductor and the reference electrode in electrolyte, Figure 1a. In other words, V_G and V_W work in tandem to control the charge density in the thin semiconductor layer. The "backside" V_G charges up the MIS stack and the "frontside" V_W charges up the electrochemical double layer, and the MIS stack and the double layer function as two capacitors coupled in series.

Our previous reports described this 4-terminal electrochemistry using 2D MoS_2, graphene, and ultrathin ZnO (< 5 nm) working electrodes and we demonstrated enhancement of both outer-sphere[1-5] and inner-sphere[6] Faradaic reaction rates. To achieve more gating power, i.e., larger electron accumulations at simultaneously lower V_G values,[7-8] we implemented high dielectric constant HfO_2 as the insulator in the MIS stack. This allowed us to achieve up to a 30-fold increase in the electron transfer rate to outer-sphere redox couples from a 5 nm ZnO back-gated electrode at V_G values less than 8 V, for example.[3] Collectively, these early demonstrations, and those of

others,[9-18] have encouraged us to continue exploring the utility of back-gated 2D working electrodes for enhancing electrochemical reaction rates.

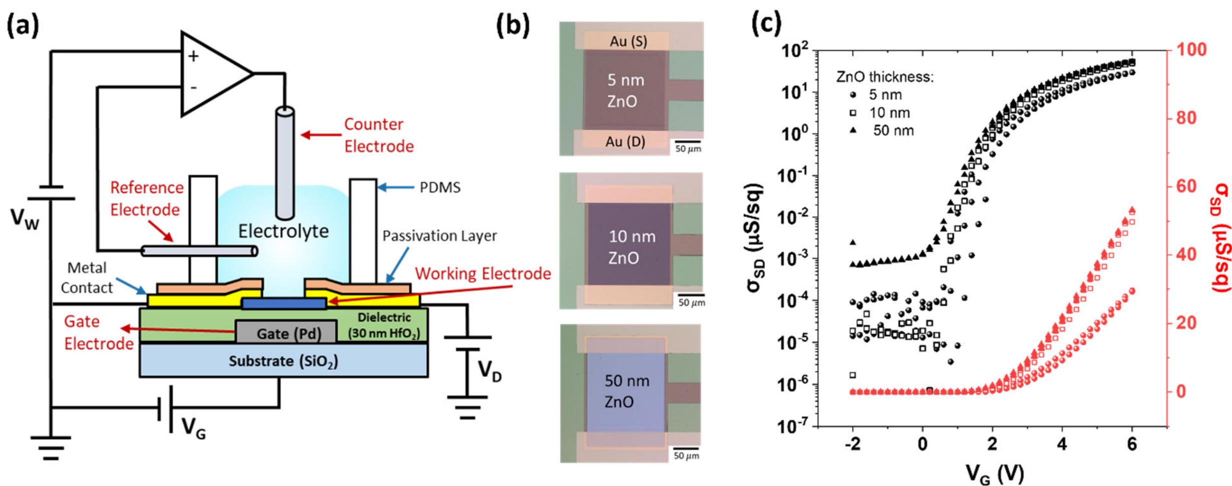

Figure 1. (a) Schematic of the four-terminal electrochemical cell with (b) optical images of the semiconductor ZnO working electrode with thicknesses of 5, 10 and 50 nm. (c) Sheet conductance of the semiconductor electrodes versus thickness and applied gate voltage (V_G), with V_G sweep rate or 0.2 V/s, and an applied V_D = 0.1 V.

Here we expand on these prior studies to further demonstrate that the 4-electrode electrochemical system serves as a platform to investigate the fundamentals of non-Faradaic electrochemical processes on semiconductors. We focus on thin back-gated ZnO electrodes, with which we have extensive experience, Figure 1. ZnO is a well-known n-type semiconductor that can be deposited with precisely controlled thicknesses in the nm regime using atomic layer deposition (ALD).[19-21] We have four principal results. First, by examining the lateral sheet conductance of the back-gated ZnO electrode in contact with electrolyte (as shown in Figure 1a) as a function of both its thickness and the applied voltages V_G and V_W, we are able estimate the ZnO thickness range where the MIS and double layer capacitors are intimately coupled. This is important because beyond this critical thickness the back gate voltage V_G will not impact electrochemistry on the top surface of the semiconductor, as will be explained. Second, by *measuring* the equilibrium electrochemical potential of the ZnO film (V_{ZnO}) as a function of V_G,

we show that V_G directly modulates the electrochemical potential of the 2D semiconductor; that is, V_G provides independent electrochemical potential control of the ZnO film, which greatly clarifies its utility. Third, we demonstrate that from measurements of V_{ZnO} vs. V_G we can extract the quantum capacitance C_Q of the ultrathin ZnO film. C_Q reflects the electronic density of states (DOS) of the semiconductor and thus this measurement serves as a kind of electronic spectroscopy. Fourth, we show that we can combine the measurements above to disentangle the two principal components of electrochemical potential, namely the Fermi level shift $\Delta\delta$ in the ZnO DOS and the double layer charging energy $e\Delta\phi_{EDL}$.[22-24] We believe that this later point will be critical in future studies of electrocatalysis where it is typically not known whether large overpotentials are mainly due to the need for a particular electron filling in the DOS (i.e., a particular $\Delta\delta$), or a certain interfacial electric field proportional to $\Delta\phi_{EDL}$. Overall, we demonstrate that back-gated working electrodes establish new opportunities to understand fundamental electronic and non-Faradaic electrochemical processes at semiconductor/electrolyte interfaces.

Materials and Methods

Materials. p^{++}-doped Si wafer with 300 nm thermally grown oxide purchased from Silicon Valley Microelectronics was used as the substrate for device fabrication. Tetrakis(dimethylamido) hafnium (TDMAH) and diethylzinc (DEZ) purchased from Sigma-Aldrich were used as the ALD precursors for growing HfO_2 (as-grown dielectric constant $k \approx 16$) and ZnO ($k \approx 8$), respectively. Sylgard 184 silicone elastomer kit (including the base and curing agent) purchased from Fisher Scientific was used to fabricate the PDMS (polydimethylsiloxane) reservoir blocks. SU8 2005 photoresist with SU8 developer (Kayaku Advanced Materials) were employed for electrode passivation. Tetrabutylammonium hexafluorophosphate (TBAP, $\geqslant$99%) and acetonitrile (MeCN,

anhydrous, 99.8%) purchased from Sigma-Aldrich were used as the electrolyte solution. Platinum wire (99.99%) with 500 µm diameter (Sigma-Aldrich) was used as the counter electrode. The Ag/Ag^+ reference electrode (BASi Co.) was filled with 10 mM $AgNO_3$ (Sigma-Aldrich) and 0.1 M TBAP in MeCN. All chemicals were used without further purification.

Device fabrication. The fabrication of the high-k local gate ZnO FET device followed procedures described in detail in prior work[3]. Briefly, a SiO_2/p-Si substrate was first pre-patterned using photolithography to achieve a local-gate structure. Next, a 20 nm thick Pd layer (on 3 nm of Cr) was deposited on the substrate using electron beam evaporation (Evaporator CHA, SEC 600) followed by lift-off to achieve the local gate electrode. The local gate structure helps to reduce leakage current and increase the breakdown strength of the devices. Next, a 30 nm layer of hafnium oxide (HfO_2) was grown as the dielectric using plasma-enhanced atomic layer deposition (PEALD) (Fiji G2). The PEALD process involved 230 cycles of alternating 250 ms pulses of tetrakis(dimethylamido)hafnium (TDMAH) and oxygen plasma (300 W) for 6 s, with nitrogen purge between the pulses. The growth temperature was 150 °C.

To avoid contamination of the interface, a layer of ZnO was immediately deposited after the HfO_2 deposition. The ZnO layer was grown using atomic layer deposition (ALD) at 200 °C for 50 cycles, 90 cycles, and 400 cycles, respectively, to achieve 5, 10, and 50 nm ZnO films (see Figure S1 in Supporting Information). Diethylzinc (DEZ) and H_2O were the precursors. Note that the 50 nm ZnO was annealed at 400 °C in O_2 for 15 min in the Rapid Thermal Annealer (RTA-600s) after deposition to achieve the desired *I-V* characteristics of the device. Annealing studies on 50 nm ZnO FETs are shown in Figure S2 in Supporting Information. The deposited ZnO film was wet etched in dilute acid solution $HCl:H_2O$ = 1:1000. After that, the HfO_2 layer was etched by plasma etching (Oxford Etcher, 180-ICP), with gas flow BCl_3:Ar at a rate of 20:5 sccm, RF

power of 100 W, and pressure of 2 mTorr, for a duration of 15 s. Finally, a layer of Ti/Au with thicknesses of 5/30 nm was deposited on the sample using electron beam evaporation, followed by a lift-off in acetone overnight. Devices with ZnO thickness of 5 nm, 10 nm and 50 nm were fabricated in this manner.

After fabrication, the front side of the device was passivated by an epoxy-based photoresist SU8 2005. The devices were patterned by photolithography with only the ZnO electrode and contact electrodes exposed. Finally, a PDMS reservoir was fabricated by curing the Sylgard 184 silicone elastomer, followed by punching a reservoir using a puncher with d = 4 mm. The PDMS reservoir was contact bonded to the device after O_2 plasma activation of the PDMS surface.

Electrochemical measurements. The 4-terminal electrochemical measurement with simultaneous back- and electrolyte-gating was performed using the configuration shown in Figure 1a. Measurements were done in ambient conditions using a probe station and a series of Keithley source measure units. A Pt wire (d = 0.5 mm) counter electrode and Ag/Ag^{+} reference electrode were used. The ZnO channel in contact with electrolyte functioned as the working electrode. A voltage (V_W) was applied between working and reference electrodes where the current flowed through the working and counter electrodes. Meanwhile, V_D was applied between source and drain electrodes and V_G was applied between the gate and source electrodes. The sheet conductance was calculated using the measured source to drain current I_D.

The configuration for electrochemical potential measurements is illustrated in Figure 4a. Here the counter electrode was not used. The working electrode was grounded, and the reference electrode was connected to a high impedance voltmeter which measured the reference potential with respect to the grounded working electrode upon sweeping V_G. In this setup, I_G and σ_{SD} can be

simultaneously measured. Before electrochemical measurements, the electrolyte solution was purged with N_2 for 15 min.

Results and Discussion

Back-gating of ZnO working electrodes with different thicknesses in the absence and presence of front-side electrolyte. Optical images of gated ZnO electrodes with film thicknesses of 5, 10, and 50 nm are shown in Figure 1b. Because there are Ti/Au source and drain contacts to each ZnO electrode, Figures 1a and 1b, the Pd/HfO_2/ZnO stack can function as a field effect transistor (FET), where the in-plane sheet conductance σ_{SD} of the ZnO film is measured as a function of V_G.[25-26] In Figure 1c, σ_{SD} is plotted vs V_G for all three ZnO thicknesses. All films are n-type, i.e., mobile electrons accumulate in ZnO with positive V_G values. Furthermore, σ_{SD} is very sensitive to V_G, increasing by up to 10^6 fold between V_G = 0 and +6 V. The higher sheet conductances in the 10 nm and 50 nm films reflect higher field effect electron mobilities ($\mu = 25$ $cm^2V^{-1}s^{-1}$) in these films than in the 5 nm ZnO films ($\mu = 15$ $cm^2V^{-1}s^{-1}$), which is perhaps be attributable to film morphology differences.

The back-gated sheet conductances of the 5, 10, and 50 nm ZnO electrodes were also measured while they were in contact with electrolyte (0.1 M TBAP in MeCN) but with no applied electrochemical potential V_W, Figure S3 in Supporting Information. The σ_{SD} vs V_G behavior of ZnO in the presence of electrolyte was similar to that shown in Figure 1c in the absence of contacting electrolyte. However, a slight increase of hysteresis was observed for 5 nm ZnO in contact with electrolyte. This is attributed to the influence of ions in the electrolyte and the formation of a weak double layer at the ZnO/electrolyte interface because of incomplete screening of the back gate field by the electronic charge in the ZnO. Electrostatically bound anions can then

interfere with electron transport in ZnO when the layer is ultrathin leading to lower currents on the backward V_G sweep. We return to this point later.

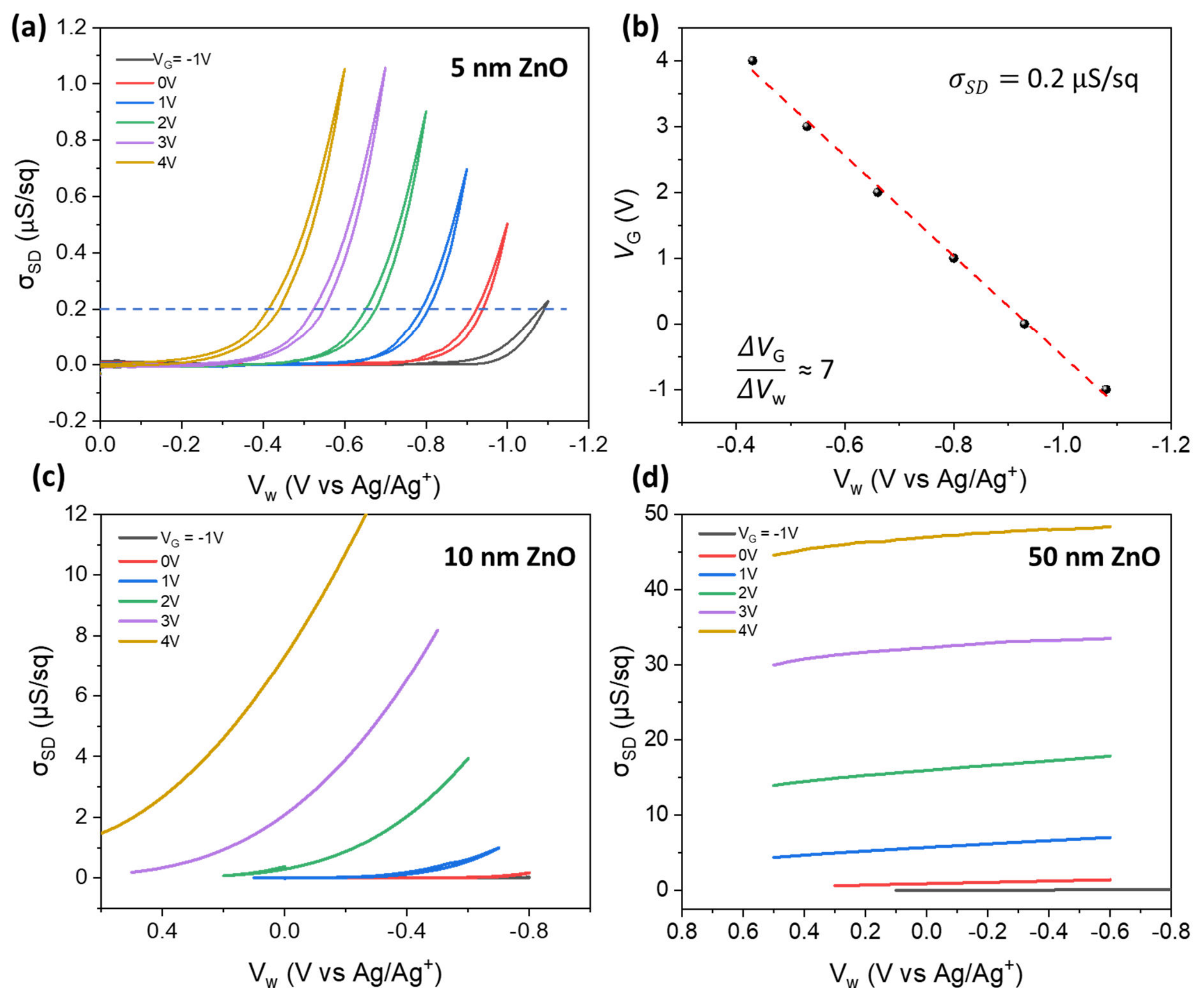

Figure 2. (a) Sheet conductance σ_{SD} of a 5 nm ZnO film as a function of V_W and V_G. Film is in contact with 0.1 M TBAP/MeCN electrolyte; V_W sweep rate is 20 mV/s, and V_D= 10 mV. (b) Plot of V_G vs V_W at a fixed σ_{SD} = 0.2 μS/sq for the 5 nm ZnO electrode (see horizontal blue dashed line in (a). The linear dependence reflects strong coupling of front and back side of the ZnO electrode. (c) and (d) σ_{SD} of 10 nm and 50 nm ZnO films, respectively, as a function of V_W and V_G.

Next we examine the in-plane σ_{SD} behavior of the ZnO electrodes, in contact with electrolyte, as a function of V_G and V_W applied simultaneously. Figure 2a displays σ_{SD} vs. V_W for a 5 nm ZnO electrode back-gated with six different values of V_G ranging from V_G = -1 V to +4V. At a given V_G value, σ_{SD} of ZnO increased as V_W was swept to negative values indicating electrons

accumulated in the ZnO at negative electrochemical potentials, as expected. Importantly, for increasingly positive V_G values, the σ_{SD} vs V_W curves systematically shifted to the left, i.e., to more positive V_W values. This means that at large V_G values, smaller (less negative) V_W bias is required to achieve the same σ_{SD}. Note that positive V_G results in electron accumulation: it is simply a difference in sign convention that $V_G > 0$ and $V_W < 0$ both correspond to electron accumulation in ZnO. Figure 2b shows the V_G vs V_W relationship explicitly; V_G is plotted vs V_W for a fixed value of the lateral sheet conductance in ZnO, i.e., σ_{ZnO} = 0.2 mS. The relationship is precisely linear and demonstrates that large V_G values mean only a small V_W is required, and vice versa, to achieve the same conductance. Selection of other σ_{SD} values would lead to a set of parallel lines on this plot.

The linear behavior in Figure 2b indicates that the front (double layer) and back (MIS) capacitors are closely coupled. This coupling can be expressed mathematically by considering a charge balance on the ZnO. At a fixed sheet conductance σ_{ZnO}, the corresponding electronic charge Q on the ZnO is the sum of charge induced across the MIS stack on the backside and the charge associated with the electrochemical double layer on the frontside. Thus,

$$Q = -V_W C_{EDL} + V_G C_G \tag{1}$$

where C_{EDL} and C_G are the double layer capacitance and HfO_2 gate dielectric capacitance, respectively. Under the assumption that fixed σ_{SD} is equivalent to fixed Q, eq. 1 predicts that the slope of the V_G vs V_W plot is C_{EDL}/C_G. We find from Figure 2b that the slope is 7 and estimating C_G = 0.6 μF/cm^2, we obtain C_{EDL} = 4.2 μF/cm^2, which is reasonable for an electric double layer.[27-28] Thus, the sheet conductance analysis for the 5 nm ZnO film is internally consistent and demonstrates that for this ultrathin ZnO layer the V_G and V_W potentials are well coupled. According to eq. 1, the linear behavior in Figure 2b also indicates that C_{EDL} and C_G are both independent of voltage.

The situation changes significantly as the ZnO electrode thickness increases. Figure 2d shows σ_{ZnO} vs V_W for the thickest 50 nm ZnO films at different V_G values. One can see that the measured σ_{ZnO} is strongly dependent on V_G, but almost completely independent of V_W; i.e., the slopes of the traces are close to zero. Stated another way, it is clear in Figure 2d that at any given V_G value, V_W is not able to shut off the sheet conductance of ZnO, whereas positive V_W values clearly caused σ_{ZnO} to collapse to near zero for the 5 nm electrode, Figure 2a. Thus, for the 50 nm electrode V_W and V_G are not strongly coupled. Figure 2c displays the intermediate case, namely the 10 nm ZnO electrode. There, increasing V_G shifts the σ_{ZnO} vs V_W curves more positive, but the overall V_W dependence is weaker than in Figure 2a, and full shut off of σ_{ZnO} at positive V_W is hard to achieve at the most positive V_G values.

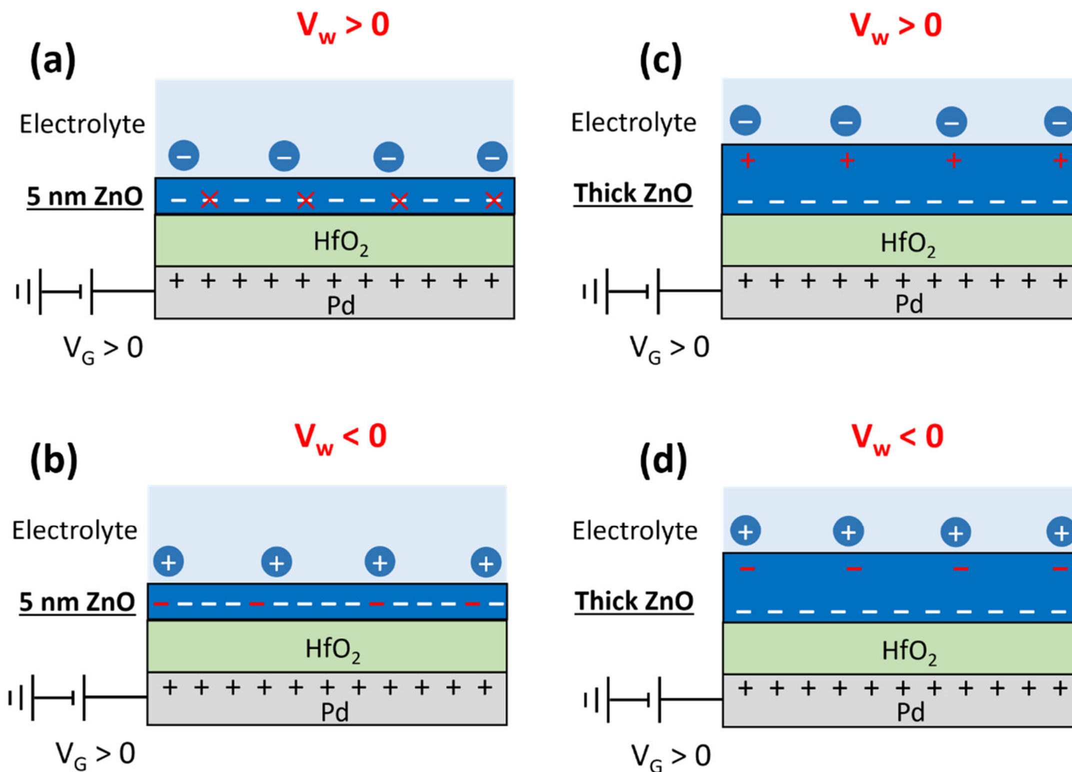

Figure 3. Scheme of charge accumulations at the ZnO/electrolyte interface under simultaneous back-gating ($V_G > 0$) and electrolyte-gating for thin, 5 nm (a, b) and thicker (c, d) ZnO electrodes. Note $V_W > 0$ for (a) and (c), and $V_W < 0$ for (b) and (d). $V_G > 0$ for all panels.

Schemes of the charge accumulation in thin and thick ZnO electrodes are depicted in Figure 3. Figure 3a shows the case where $V_G > 0$ and $V_W > 0$. In this case the backside gate induces electrons in 5 nm ZnO, but the electrochemical (double layer) gate depletes electrons. The two competing processes lead to reduced electron density in the 5 nm ZnO compared to the application of V_G alone. Figure 3b depicts the case where $V_G > 0$ and $V_W < 0$. Now the front and back gates work together to boost the net electron density in the 5 nm ZnO film beyond what can be accumulated by V_G alone. These scenarios rationalize the data shown in Figure 2a for ultrathin 5 nm ZnO films.

On the other hand, Figures 3c and 3d show the expected situations for 50 nm thick ZnO films. One can see in Figures 3c and 3d that the charges induced by the electrical double layer (shown in red) are spatially separated from the charges induced by the back gate (shown in white). The front and back capacitors are decoupled and this means that V_W has little influence on the accumulated electron density induced by V_G. Stated another way, there is no depletion of mobile electrons for any positive value of V_W and one predicts that the sheet conductance is weakly affected by V_W, which is what we observe in Figure 2d.

Determining the ZnO equilibrium potential (V_{ZnO}) vs V_G and quantum capacitance (C_Q). Next, instead of *applying* the working electrode potential V_W, we *measured* the electrochemical potential on ZnO electrodes (denoted as V_{ZnO}) with respect to the reference (Ag/Ag^+) while sweeping V_G. Figure 4a shows V_{ZnO} vs V_G data for a 5 nm thick ZnO electrode and the electrical setup for this measurement is depicted in the inset. The first observation in Figure 4a is that for a V_G range of -1 V to +6 V, or 7 V total, V_{ZnO} varies by nearly 1 V from +0.55 V to -0.4 V vs Ag/Ag^+. This is a critical result: it says that V_G provides direct control of the electrochemical potential of the thin ZnO film, and that *large* changes in electrochemical potential, of order 1 V, are accessible

by means of back-gating. The second observation is that two domains are evident in the Figure 4a plot. At low V_G values, V_{ZnO} increases strongly (becomes more negative) with increasing V_G. However, near V_G = +1.5 V there is a slope change. For V_G > +1.5 V, V_{ZnO} continues to become more negative, but it does so more slowly.

It can be shown (see Supporting Information) that the slope of the V_{ZnO} vs V_G plot is directly related to the capacitance of the HfO_2 dielectric C_G and the quantum capacitance C_Q of the ZnO film:

$$\frac{dV_{ZnO}}{dV_G} = -\frac{1}{1+\frac{C_Q}{C_G}} \quad (2)$$

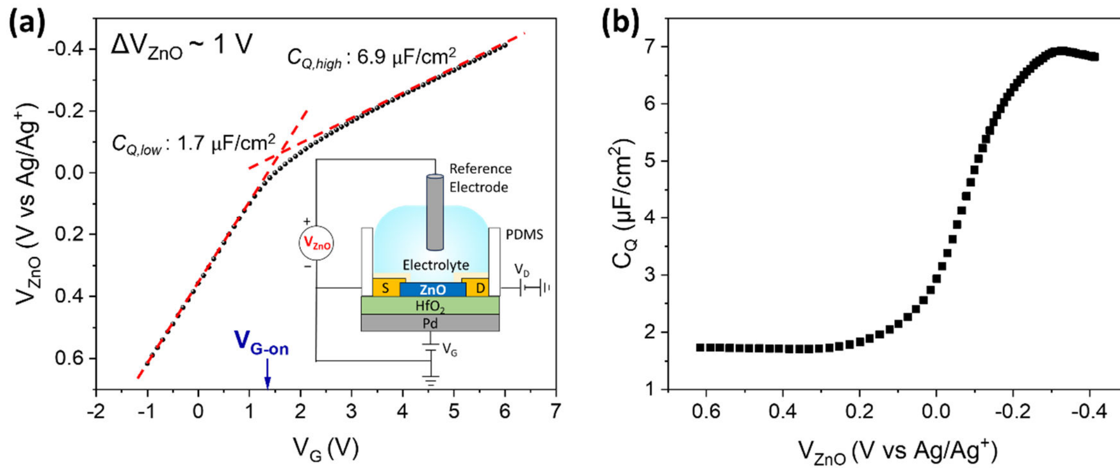

Figure 4. (a) Electrochemical potential V_{ZnO} of a 5 nm ZnO electrode with respect to the Ag/Ag^+ reference electrode measured while back-gating, using the setup shown in the inset. The V_G sweep rate is 1V/s. The red dashed lines are fits to the data using eq. 2 and show the change of slope before and after the device turned on. (b) Quantum capacitance C_Q vs V_{ZnO} obtained from the data in (a) using eq. 2.

C_Q is the intrinsic capacitance of a material due to its electronic density of states ($C_Q = e^2 \cdot$ DOS).[29-31] For typical metal/insulator/metal capacitors, $C_Q^{metal} >> C_G^{insulator}$ and the derivative in Eq. 2 is effectively zero. However, for an ultrathin film semiconductor on a high capacitance dielectric, C_G can be the same order of magnitude as C_Q. This is the situation here. C_G^{HfO2}= 0.6 μF/cm^2, which is

a large value fixed by the dielectric constant and thickness of the HfO_2 layer. From straight line fits to the two domains in Figure 4a, we extract $C_{Q,low}^{ZnO}$= 1.7 μF/cm^2 and $C_{Q,high}^{ZnO}$= 6.9 μF/cm^2 using eq. 2. The abrupt slope change evident in Figure 4a is caused by an abrupt change in C_Q^{ZnO} at approximately V_G = +1.5 V, or V_{ZnO} ~ 0 V vs Ag/Ag$^+$. Figure 4b displays the continuous variation in C_Q^{ZnO} vs V_{ZnO} obtained from panel (a) using equation 2. It is clear that there is a step change in C_Q^{ZnO} as V_{ZnO} is varied.

We can understand the changes in C_Q^{ZnO} in this way. At low V_G values the Fermi level E_F of the ZnO film is deep in the ZnO band gap where the density of electronic states (DOS) should be low (the only in-gap states are localized trap states). As V_G swings positive the field effect causes the conduction band edge to shift down, or equivalently in the language of electrochemists one can say the Fermi level moves up toward the conduction band edge. Because the DOS is low, C_Q^{ZnO} is low, and small changes in V_G produce relatively large gains in V_{ZnO}. However, once the conduction band to E_F offset (δ) becomes small enough, the channel opens, electrons accumulate in the conduction band, and the DOS near E_F is much higher. Consequently, C_Q^{ZnO} is higher. This means that beyond V_G = +1.5 V, V_{ZnO} is less sensitive to V_G (i.e., more electrons can accumulate at a given energy because the DOS is high). We note that the σ_s vs V_G plot in Figure 1c also shows that the threshold voltage V_T for onset of conduction is ~+1.5 V; Figure 1c is consistent with the data in Figures 4a and b.

Separating band edge shift $\Delta\delta$ from double layer charging energy e$\Delta\phi_{EDL}$. We have shown above that the back gate controls electrochemical potential of the ZnO film. In this last section we consider the fundamental differences between back-gating and normal electrochemical gating in our 4 electrode cell.

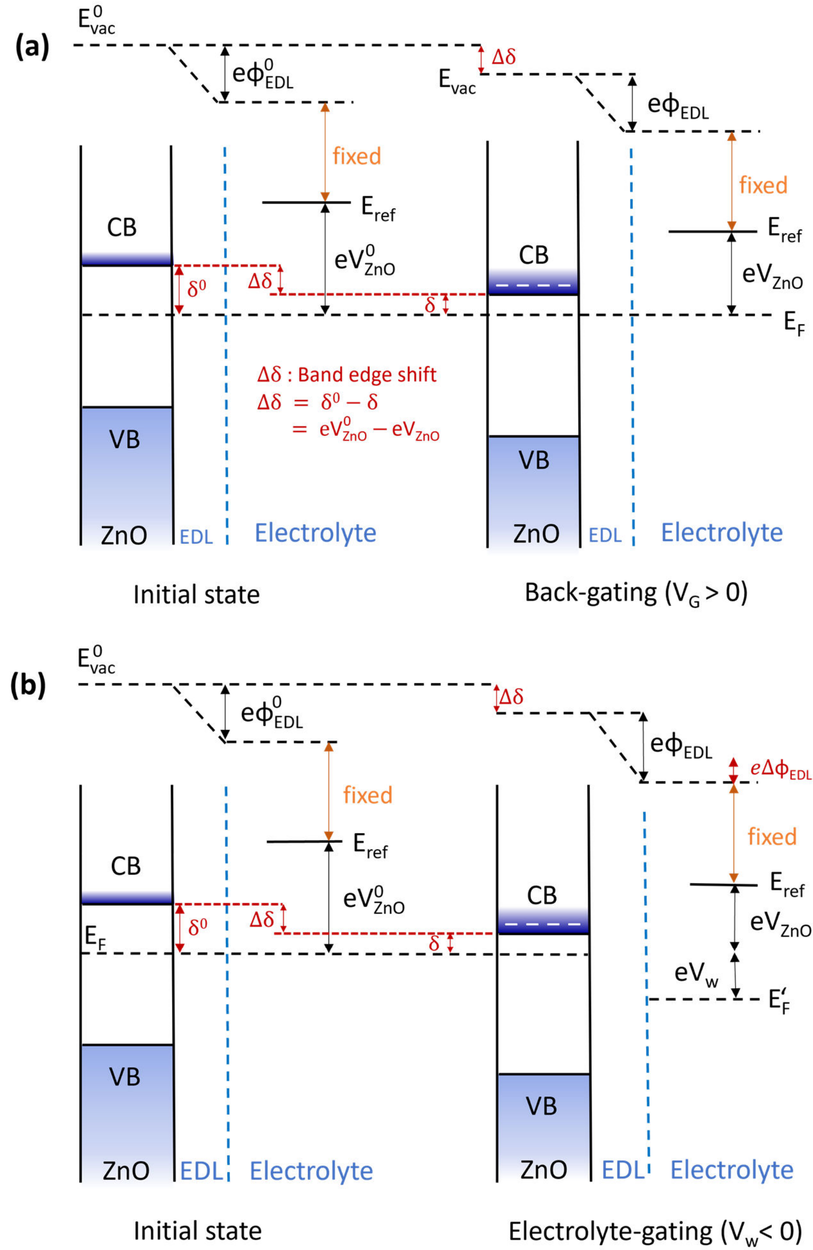

Figure 5. Energy level diagram for the ultrathin ZnO electrode/electrolyte interface. (a) The initial and final states under back-gating where $V_G > 0$ V is applied across the Pd/HfO_2/ZnO capacitor. The voltage drop across the MIS capacitor is not shown; only the ZnO/electrolyte interface is shown. (b) The initial and final states for front-side electrochemical gating with $V_W < 0$. In both (a) and (b), δ^0 and δ are the conduction band offsets from the Fermi level E_F in the initial state and final states, respectively; $\Delta\delta$ is the band edge shift; V^0_{ZnO} and V_{ZnO} are the equilibrium potentials of ZnO versus the reference E_{ref}; ϕ_{EDL} is the double layer potential; E^0_{vac} is the vacuum level. Blue shading in the conduction bands (CB) and valence bands (VB) indicates the electron energy distribution.

Figures 5a and b depict energy level diagrams for back-gating and front-side electrochemical gating, respectively. Considering Figure 5a first, application of a back gate voltage V_G pulls the conduction band edge down towards the system Fermi level E_F via the field effect. The initial offset between the conduction band and E_F is δ^0 (see "initial state" in Figure 5a). Application of $V_G > 0$ shrinks the band edge offset from δ^0 to δ. E_F is fixed across the whole system because the ZnO film and the reference electrode are in equilibrium ($V_W = 0$).

The band edge shift is given by the difference in band edge position before and after V_G is applied, i.e., $\Delta\delta = \delta^0 - \delta$. Correspondingly, V_{ZnO} measures the position of E_F relative to the fixed Ag/Ag^+ reference is shown. Initially, the electrochemical potential is V_{ZnO}^0. Upon back-gating the equilibrium potential shifts to V_{ZnO}. From the diagram one can work out that

$$\Delta\delta = \delta^0 - \delta = e(V_{ZnO}^0 - V_{ZnO}) \quad (3)$$

Eq. 3 expresses the important idea that the equilibrium electrochemical potential V_{ZnO} can be used to measure the band edge shift $\Delta\delta$. The significance of $\Delta\delta$ is that it determines the electron density in the conduction band via the DOS and the Fermi function; small $\Delta\delta$ means large electron accumulations.

Turning now to the electrochemical gating picture in Figure 5b, $V_G = 0$ but $V_W < 0$. Negative V_W brings cations to the ZnO/electrolyte interface as electrons accumulate on the ZnO, charging up the double layer. Charging the double layer has two effects: (i) it results in an increase in the double layer potential drop $\Delta\phi_{EDL} = \phi_{EDL} - \phi'_{EDL}$ between the initial final states, and (ii) it causes the conduction band edge to shift down by $\Delta\delta$. Using an energy balance, we can capture these two effects mathematically:[32-34]

$$eV_W = \Delta\delta + e\Delta\phi_{EDL} \quad (4)$$

That is, the energy provided by the external circuit supplying eV_W is the sum of the band edge shift for ZnO and the double layer charging energy. In Figure 5b E_F is not constant across the semiconductor/electrolyte interface because of the applied electrochemical potential V_W.

For comparison, we can write a similar equation for back-gate charging, i.e.,

$$eV_G = \Delta\delta + e\Delta\phi_{dielectric} \quad (5)$$

where $e\Delta\phi_{dielectric}$, which is not depicted in Figure 5, is the energy invested in polarizing the insulator layer in the MIS stack. We see in eqs. 4 and 5 the symmetry of the back-gate and conventional electrochemical control: in both cases the supplied electrical energy produces band edge shifts and material polarization (double layer vs. dielectric). A critical point, however, is that for back-gating we can isolate $\Delta\delta$ in eq. 5 via measurements of V_{ZnO} and eq. 3, and so we can directly compare $\Delta\delta$ and $e\Delta\phi_{dielectric}$ for a given V_G. At first glance it seems that we do not have the same opportunity to know the relative magnitudes of $\Delta\delta$ and $e\Delta\phi_{EDL}$ in eq. 4, because we do not have independent measures of either $\Delta\delta$ or $e\Delta\phi_{EDL}$.

However, it turns out that we can indeed disentangle $\Delta\delta$ and $e\Delta\phi_{EDL}$ using two distinct experiments. In the first experiment we measure the in-plane sheet conductance σ_{SD} of ZnO vs V_W (i.e., applied electrochemical potential), keeping V_G = 0 V. In the second experiment, we measure both σ_{SD} and the equilibrium electrochemical potential V_{ZnO} of the ZnO film while sweeping V_G. Plots of σ_{SD} vs V_W and σ_{SD} vs V_{ZnO} are then overlaid. Because V_W and V_{ZnO} are on the same scale – i.e., one is applied electrochemical potential and the other is measured equilibrium potential versus the same reference – the x-axes are interchangeable. Figure 6 shows example data. The two curves have been shifted to align the sheet conductances just at channel turn on. One sees in Figure 6 that a higher potential is required in the red trace (electrochemical gating only) to achieve the same σ_{SD} as in the black trace (back-gating only). The reason is that σ_{SD} in the black trace hinges only

on the band offset change $\Delta\delta$, which sets the electron distribution in ZnO. For the red trace, on the other hand, the potential at the same σ_{SD} value reflects the sum of $\Delta\delta/e$ and $\Delta\phi_{EDL}$(eq. 4). Making the reasonable assumption that $\Delta\delta$ is the same for the two traces at the same $\sigma_{SD} = 0.1$ µS (this is equivalent to saying that the electron densities in ZnO are the same), we can take the shift in energy along the x-axis to be an approximate measure of $\Delta\phi_{EDL}$, as shown. Importantly, one sees that $\Delta\phi_{EDL}$ is similar in magnitude to $\Delta\delta/e$, i.e., $\Delta\phi_{EDL} \approx \Delta\delta/e \approx 0.1$ V. In other words, for electrochemical gating about half the electrochemical energy in the applied V_W is spent on charging the double layer.

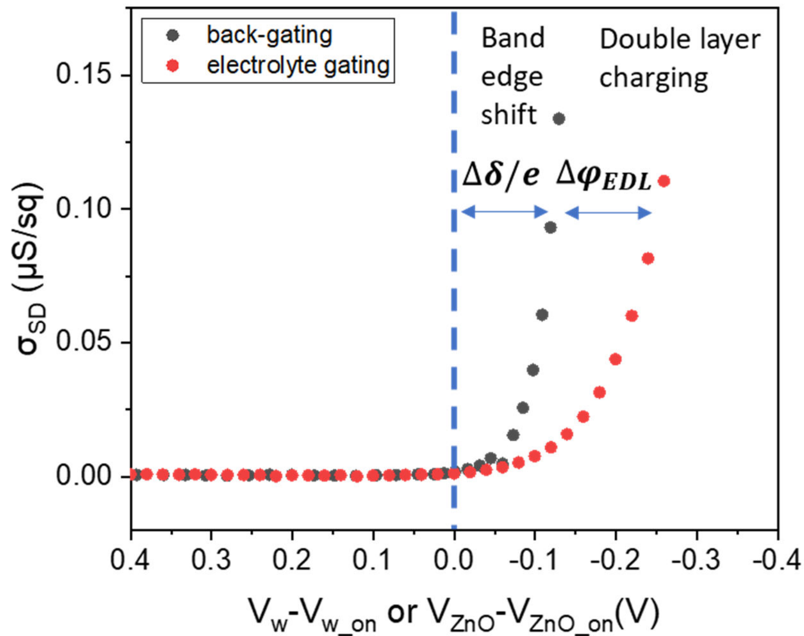

Figure 6. Sheet conductance of the 5 nm thick ZnO electrode versus electrochemical potential for two different experiments. In one experiment (red trace), the sheet conductance was measured versus the working electrode potential, V_W. In the second experiment, sheet conductance and the electrochemical potential V_{ZnO} of the ZnO were measured simultaneously while the back gate potential V_G was swept. The black trace is thus the measured sheet conductance versus the measured electrochemical potential V_{ZnO} during back gating. It is evident that a smaller change in the electrochemical potential of the ZnO is required to achieve the same sheet conductance when back gating versus normal potential control. This is because back gating does not require full double layer charging to achieve the same electron density, i.e., conductance. Note that the two traces were aligned at V_{w_on} and V_{ZnO_on} which are the potentials corresponding to the onset of electron conduction.

We note that the values extracted from Figure 6 are approximate and subject to assumptions underlying eq. 3. Eq 3 states that $e\Delta V_{ZnO} = \Delta\delta$, but this is only true if back-gating does not result in any double layer charging at the ZnO/electrolyte interface. If the ZnO screening length at a given electron concentration is larger than the thickness of ZnO, some back gate field lines will penetrate through the ZnO into the electrolyte where they will attract anions. In such a case the measured V_{ZnO} will be larger than the actual $\Delta\delta/e$. Thus, $\Delta\delta/e$ will be overestimated by eq. 3. Returning to our Figure 6 analysis, $\Delta\delta/e$ depicted is an upper limit, which means that $\Delta\phi_{EDL}$ could be somewhat larger than indicated. More experiments are necessary to determine exactly what the ZnO thickness should be to have complete gate field screening in the ZnO and no anion attraction (i.e., electric double layer formation). Our sheet conductance measurements on 5 nm ZnO showed some hysteresis that we attributed to ion motion at the interface (Figure S3). Still, Figure 6 illustrates an important point, namely that $\Delta\delta/e$ and $\Delta\phi_{EDL}$ can be deconvoluted in principle. We speculate that in future experiments on electrocatalysis, one may be able to compare plots of reaction current versus V_W and V_{ZnO} simultaneously to assess the relative importance of $\Delta\delta/e$ vs $\Delta\phi_{EDL}$ to the required overpotential.

Conclusion

In conclusion, we have shown that the electrochemical potential (E_F position in the DOS) of a 5 nm thick ZnO semiconductor working electrode can be varied by nearly 1 V vs an Ag/Ag^+ reference electrode by application of a 7 V gate bias between the ZnO and a capacitively coupled gate electrode. The gate bias V_G thus acts as an independent control of the working electrode electrochemical potential that acts in tandem with the conventional electrochemical potential V_W. We have exploited this independent control in a 4-terminal setup to make measurements of the

quantum capacitance C_Q of the ZnO film as a function of Fermi level position, a measurement that is difficult to achieve with a normal 3-terminal experiment because of the convolution of double layer charging potential $\Delta\phi_{EDL}$ with the Fermi level shift potential $\Delta\delta/e$. We anticipate that C_Q measurements, which represent a kind of spectroscopy, could be used to characterize the DOS of a variety of ultrathin semiconductor films as has been reported for certain 2D materials. We have also used the 4-terminal setup to explicitly deconvolute $\Delta\phi_{EDL}$ and $\Delta\delta/e$ for different charge states of the ZnO electrode. Overall, ultrathin back-gated working electrodes appear promising for fundamental understanding of the electronic and non-Faradaic electrochemical processes occurring at semiconductor/electrolyte interfaces.

Supporting Information

ALD thin film growth, electronic measurements on ZnO FETs, derivation of equations

Acknowledgements

This work was primarily supported by the Department of Energy, Basic Energy Sciences Catalysis Program (DE-SC0021163). Parts of the work was carried out in the Characterization Facility at University of Minnesota, which was partially supported by the NSF through the MRSEC program (DMR-2011401). Other portions of this work were conducted in the Minnesota Nano Center, which is supported by the National Science Foundation through the National Nano Coordinated Infrastructure Network (NNCI) under Award Number ECCS-2025124.

References

1. Kim, C. H.; Frisbie, C. D. Field Effect Modulation of Outer-Sphere Electrochemistry at Back-Gated, Ultrathin Zno Electrodes. *J. Am. Chem. Soc.* **2016,** *138* (23), 7220-3.
2. Wang, Y.; Kim, C.-H.; Yoo, Y.; Johns, J. E.; Frisbie, C. D. Field Effect Modulation of Heterogeneous Charge Transfer Kinetics at Back-Gated Two-Dimensional MoS_2 Electrodes. *Nano Lett.* **2017,** *17* (12), 7586-7592.
3. Wang, Y.; Wang, Y.; Frisbie, C. D. Electrochemistry at Back-Gated, Ultrathin ZnO Electrodes: Field-Effect Modulation of Heterogeneous Electron Transfer Rate Constants by 30× with Enhanced Gate Capacitance. *ACS Applied Materials & Interfaces* **2023,** *15* (7), 9554-9562.
4. Kim, C. H.; Frisbie, C. D. Determination of Quantum Capacitance and Band Filling Potential in Graphene Transistors with Dual Electrochemical and Field-Effect Gates. *J. Phys. Chem. C* **2014,** *118* (36), 21160-21169.
5. Kim, C. H.; Wang, Y.; Frisbie, C. D. Continuous and Reversible Tuning of Electrochemical Reaction Kinetics on Back-Gated 2D Semiconductor Electrodes: Steady-State Analysis Using a Hydrodynamic Method. *Anal. Chem.* **2019,** *91* (2), 1627-1635.
6. Wang, Y.; Udyavara, S.; Neurock, M.; Frisbie, C. D. Field Effect Modulation of Electrocatalytic Hydrogen Evolution at Back-Gated Two-Dimensional MoS_2 Electrodes. *Nano Lett.* **2019,** *19* (9), 6118-6123.
7. Shim, J. H.; Choi, H. J.; Kim, Y.; Torgersen, J.; An, J.; Lee, M. H.; Prinz, F. B. Process-Property Relationship in High-K ALD $SrTiO_3$ and $BaTiO_3$: A Review. *J. Mater. Chem. C* **2017,** *5* (32), 8000-8013.
8. Ortiz, R. P.; Facchetti, A.; Marks, T. J. High-K Organic, Inorganic, and Hybrid Dielectrics for Low-Voltage Organic Field-Effect Transistors. *Chem. Rev.* **2010,** *110* (1), 205-239.
9. Yang, H.; He, Q.; Liu, Y.; Li, H.; Zhang, H.; Zhai, T. On-Chip Electrocatalytic Microdevice: An Eemerging Platform for Expanding the Insight into Electrochemical Processes. *Chem. Soc. Rev.* **2020,** *49* (10), 2916-2936.
10. He, Y.; He, Q.; Wang, L.; Zhu, C.; Golani, P.; Handoko, A. D.; Yu, X.; Gao, C.; Ding, M.; Wang, X. Self-Gating in Semiconductor Electrocatalysis. *Nat. Mater.* **2019,** *18* (10), 1098-1104.
11. Wang, J.; Yan, M.; Zhao, K.; Liao, X.; Wang, P.; Pan, X.; Yang, W.; Mai, L. Field Effect Enhanced Hydrogen Evolution Reaction of MoS_2 Nanosheets. *Adv. Mater.* **2017,** *29* (7), 1604464.
12. Wu, Y.; Ringe, S.; Wu, C. L.; Chen, W.; Yang, A.; Chen, H.; Tang, M.; Zhou, G.; Hwang, H. Y.; Chan, K., et al. A Two-Dimensional MoS_2 Catalysis Transistor by Solid-State Ion Gating Manipulation and Adjustment (Sigma). *Nano Letters* **2019,** *19* (10), 7293-7300.
13. Pan, Y.; Wang, X.; Zhang, W.; Tang, L.; Mu, Z.; Liu, C.; Tian, B.; Fei, M.; Sun, Y.; Su, H., et al. Boosting the Performance of Single-Atom Catalysts Via External Electric Field Polarization. *Nat. Commun.* **2022,** *13* (1), 3063.
14. Ding, M.; He, Q.; Wang, G.; Cheng, H. C.; Huang, Y.; Duan, X. An on-Chip Electrical Transport Spectroscopy Approach for in Situ Monitoring Electrochemical Interfaces. *Nat. Commun.* **2015,** *6* (1), 1-9.
15. Chen, J.; Lu, N.; Zhao, Y.; Huang, J.; Gan, X.; Chen, X.; Yang, Z.; Wen, Q.; Zhai, T.; Liu, Y. On-Chip Microdevice Unveils Reactant Enrichment Effect Dominated Electrocatalysis Activity in Molecular-Linked Catalysts. *Nano Letters* **2022,** *22* (24), 10154-10162.
16. Qi, J.; Wang, W.; Li, Y.; Sun, Y.; Wu, Z.; Bao, K.; Wang, L.; Ye, R.; Ding, M.; He, Q. On-Chip Investigation of Electrocatalytic Oxygen Reduction Reaction of 2d Materials. *Small* **2022,** *18* (47), 2204010.
17. Zhao, Y.; Huang, J.; Chen, J.; Gan, X.; Wen, Q.; Li, H.; Duan, J.; Chen, B.; Zhai, T.; Liu, Y. External-Field-Driven Molecular Polarization Manipulates Reactant Interface toward Efficient Hydrogen Evolution. *Science China Materials* **2023,** *66* (9), 3501-3508.
18. Wang, J.; Qiu, M.; Jiang, Y.; Xia, H.; An, X.; Wang, S.; He, Y. Emerging on-Chip Microcells in Electrocatalysis: Functions of Window and Circuit. *EES Catal.* **2023,** *1*, 874-891.
19. Carcia, P. F.; McLean, R. S.; Reilly, M. H. High-Performance Zno Thin-Film Transistors on Gate Dielectrics Grown by Atomic Layer Deposition. *Applied Physics Letters* **2006,** *88* (12), 123509.

20. Lim, S. J.; Kwon, S.; Kim, H. ZnO Thin Films Prepared by Atomic Layer Deposition and RF Sputtering as an Active Layer for Thin Film Transistor. *Thin Solid Films* **2008,** *516* (7), 1523-1528.
21. Tynell, T.; Karppinen, M. Atomic Layer Deposition of ZnO: A Review. *Semicond. Sci. Technol.* **2014,** *29* (4), 043001.
22. Nozik, A. J.; Memming, R. Physical Chemistry of Semiconductor-Liquid Interfaces. *J. Phys. Chem.* **1996,** *100* (31), 13061-13078.
23. Bard, A. J. F., L. R. Electrochemical Methods: Fundamentals and Applications; 2nd Ed.;. *Wiley: New York,* **2006**.
24. Morrison, S. R., *Electrochemistry at Semiconductor and Oxidized Metal Electrodes*. Plenum Press,New York, NY: United States, 1980.
25. Zaumseil, J.; Sirringhaus, H. Electron and Ambipolar Transport in Organic Field-Effect Transistors. *Chemical Reviews* **2007,** *107* (4), 1296-1323.
26. Choi, H. H.; Cho, K.; Frisbie, C. D.; Sirringhaus, H.; Podzorov, V. Critical Assessment of Charge Mobility Extraction in Fets. *Nat. Mater.* **2018,** *17* (1), 2-7.
27. Wu, J. Understanding the Electric Double-Layer Structure, Capacitance, and Charging Dynamics. *Chemical Reviews* **2022,** *122* (12), 10821-10859.
28. Li, D. D.; Li, E. C.; Yang, Y. R.; Wang, X. D.; Feng, G. Structure and Capacitance of Electrical Double Layers in Tricationic Ionic Liquids with Organic Solvents. *The Journal of Physical Chemistry B* **2021,** *125* (46), 12753-12762.
29. Dröscher, S.; Roulleau, P.; Molitor, F.; Studerus, P.; Stampfer, C.; Ensslin, K.; Ihn, T. Quantum Capacitance and Density of States of Graphene. *Applied Physics Letters* **2010,** *96* (15), 152104.
30. Berthod, C.; Zhang, H.; Morpurgo, A. F.; Giamarchi, T. Theory of Cross Quantum Capacitance. *Physical Review Research* **2021,** *3* (4), 043036.
31. Liang, Y.; Chang, H. C.; Paul Ruden, P.; Daniel Frisbie, C. Examination of Au, Cu, and Al Contacts in Organic Field-Effect Transistors Via Displacement Current Measurements. *Journal of Applied Physics* **2011,** *110* (6), 064514.
32. Abbas, G.; Sonia, F. J.; Jindra, M.; Červenka, J.; Kalbáč, M.; Frank, O.; Velický, M. Electrostatic Gating of Monolayer Graphene by Concentrated Aqueous Electrolytes. *The Journal of Physical Chemistry Letters* **2023,** *14* (18), 4281-4288.
33. Das, A.; Pisana, S.; Chakraborty, B.; Piscanec, S.; Saha, S. K.; Waghmare, U. V.; Novoselov, K. S.; Krishnamurthy, H. R.; Geim, A. K.; Ferrari, A. C., et al. Monitoring Dopants by Raman Scattering in an Electrochemically Top-Gated Graphene Transistor. *Nat. Nanotechnol.* **2008,** *3* (4), 210-215.
34. Froehlicher, G.; Lorchat, E.; Berciaud, S. Charge Versus Energy Transfer in Atomically Thin Graphene-Transition Metal Dichalcogenide Van Der Waals Heterostructures. *Phys. Rev. X* **2018,** *8* (1), 011007.

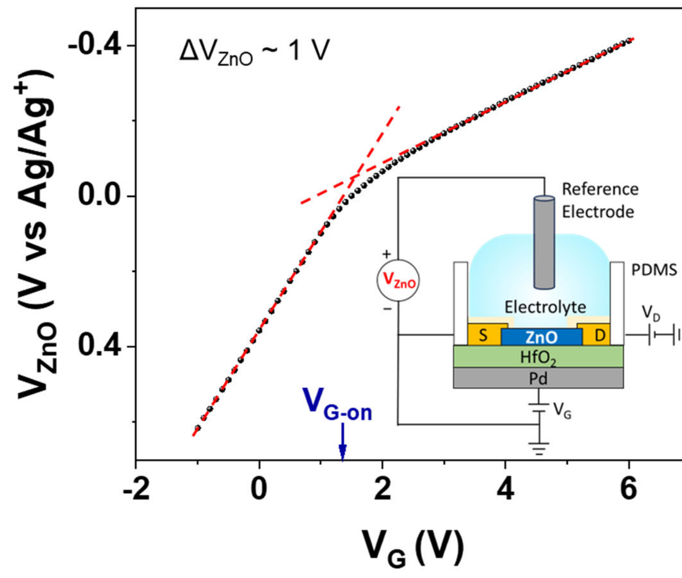

TOC graph